

Creating currents of electric bubbles

Jorge Íñiguez-González^{1,2} and Hugo Aramberri¹

¹Luxembourg Institute of Science and Technology (LIST), Avenue des Hauts-Fourneaux 5, L-4362 Esch/Alzette, Luxembourg

²Department of Physics and Materials Science, University of Luxembourg, Rue du Brill 41, L-4422 Belvaux, Luxembourg

The experimental demonstration of electric skyrmion bubbles and the recent prediction of their Brownian motion have brought topological ferroelectrics close to their magnetic counterparts. Electric bubbles (e-bubbles) could potentially be leveraged in applications for which magnetic skyrmions have been proposed (e.g., neuromorphic computing). Yet, we still lack a strategy to create currents of e-bubbles. Here, using predictive atomistic simulations, we illustrate two approaches to induce e-bubble currents by application of suitable electric fields, static or dynamic. We focus on regimes where e-bubbles display spontaneous diffusion, which allows us to generate a current by simply biasing their Brownian motion. Our calculations indicate that e-bubble velocities over 25 m/s can be achieved at room temperature, suggesting that these electric quasiparticles could rival the speeds of magnetic skyrmions upon further optimization.

Recent studies have addressed the possibility of stabilizing and manipulating electric bubbles (e-bubbles) [1–5], evidenced their nontrivial topologies [6–8], and even predicted their behavior as Brownian quasiparticles [9]. Perovskites are the best studied materials, with ferroelectric/dielectric PbTiO₃/SrTiO₃ superlattices (PTO/STO) emerging as model systems [10].

The prediction that e-bubbles can display spontaneous stochastic diffusion resonates with novel computing concepts that leverage thermal noise and the associated randomness [11–14]. Ultralow-power devices based on Brownian magnetic skyrmions have been proposed, and functionalities ranging from non-linearly separable XOR operations [15, 16] to pattern recognition [17] demonstrated. These schemes fall within the category of “unconventional computing”, a promising path toward sustainable artificial intelligence [18]. In this context, e-bubbles controllable by electric fields – as opposed to the electric currents needed to act on magnetic skyrmions – may enable more efficient devices.

To fulfill this promise, though, we must improve our understanding of e-bubbles and, in particular, address their mobility. Since 2010 we know that small electric currents can be used to move magnetic skyrmions [19, 20]. Can something equivalent be done with e-bubbles? Here we give a positive answer to this question, presenting simulation evidence for e-bubble currents driven by suitable electric fields.

We work with PTO/STO superlattices where e-

bubbles have been observed [6, 9], using the atomistic “second-principles” simulation techniques [21, 22] that have successfully predicted the main properties of these materials [6, 7, 23, 24]. (See Methods for details.) A compressive epitaxial strain in the xy plane, e.g. as imposed by a STO substrate, yields an easy polar axis along the stacking direction z . Further, the dielectric STO layers impose open-circuit-like electric boundary conditions on the PTO layers, which develop ferroelectric stripe domains with $P_z = 0$ overall. If an electric field is applied along z , the stripes break and e-bubbles form [9]. Typically, the bubbles span the whole thickness of the PTO layer and have an approximately circular xy section a few nanometers in diameter.

In ultrathin PTO layers (below 10 unit cells) the bubbles have a small surface, which suggests that thermal fluctuations may result in a net drift of the whole object. Indeed, simulations predict that – within a range of about 100 K below the Curie point – e-bubbles diffuse spontaneously [9, 25], an effect consistent with XRD data [22]. The bubbles are predicted to remain stable even when diffusing, behaving as long-lived Brownian particles [9].

This leads to a self-evident notion: if we create an asymmetry in the xy plane, the Brownian diffusion must yield a net bubble current. Indeed, following similar ideas, a temperature gradient was used to move magnetic skyrmions [26]. Here we use electric fields to drive the effect, as they are an experimentally convenient choice.

Let us first show how to induce a current of e-bubbles by applying a static position-dependent electric field. We apply a z -oriented homogeneous field $\mathcal{E}_z^{(0)}$ to create bubbles in the PTO layers. Assume $\mathcal{E}_z^{(0)} > 0$, so the bubbles correspond to regions of downward polarization within a matrix polarized upward. Now consider a linear spatial dependence of the total field,

$$\mathcal{E}_{\text{tot},z}(x) = \mathcal{E}_z^{(0)} + \mathcal{E}_z^{(1)} \frac{2x - L}{2L}, \quad (1)$$

where L is a characteristic length of our simulated system, $\mathcal{E}_z^{(1)}/L$ quantifies a field gradient, and we assume $\mathcal{E}_z^{(1)} > 0$. If we approximate the bubble as a point dipole $d_{b,z} < 0$, its energy under this field is given by $V_b \approx -\mathcal{E}_{\text{tot},z} d_{b,z}$. The bubble thus experiences a force

$$f_{b,x} = -\frac{\partial V_b}{\partial x} = \frac{\mathcal{E}_z^{(1)} d_{b,z}}{L} < 0, \quad (2)$$

which drives it toward smaller x values. Hence, in principle, a field gradient may allow us to move e-bubbles.

To test this, we run simulations of PTO/STO superlattices that we denote 9/3 and 6/3 – i.e., where the STO layers have a thickness of 3 elemental perovskite cells, while the PTO layers have thicknesses of 9 and 6 cells, respectively. We work in conditions where long-lived Brownian bubbles were previously predicted [9], namely, with the 9/3 superlattice at around 300 K and subject to a -2% compressive epitaxial strain, and with the 6/3 system at around 200 K and a 0% epitaxial strain. (The STO lattice constant is taken as the zero of strain.) We consider simulation supercells that can be seen as an $N \times 8 \times 1$ repetition of the elemental superlattice unit, and impose periodic boundary conditions. While we consider N values between 8 and 32, most of our results are for $N = 8$, which proves sufficient. The applied $\mathcal{E}_z^{(0)}$ fields are chosen to stabilize a single e-bubble in the $8 \times 8 \times 1$ supercell; we find this can be done for $\mathcal{E}_z^{(0)}$ around 1.0 MV cm^{-1} and 1.5 MV cm^{-1} , respectively, for the 9/3 and 6/3 systems.

As sketched in Figure 1a, the use of periodic boundary conditions forces us to apply a sawtooth-modulated field, rather than a homogeneous gradient. This field is given by Eq. (1) for $0 < x < L$, where L is the length of the simulation supercell along x , and it is periodically repeated for $x < 0$ and $x > L$. Thus, $\mathcal{E}_z^{(1)}$ quantifies the field change across one supercell period. Typically we consider $\mathcal{E}_z^{(1)}$ values within 20% of the homogeneous component $\mathcal{E}_z^{(0)}$; such perturbations do not change the bubble density in our supercell.

We run molecular dynamics (MD) simulations to study the equilibrium state of these systems. (See Methods for details.) In particular, we compute $\mathcal{P}(x)$, the probability of finding the bubble centered at x . Figures 1b and 1c summarize our results. We find that the bubble is largely restrained to the left half of the simulation supercell. As expected, the confinement is stronger as $\mathcal{E}_z^{(1)}$ increases (Fig. 1b) and at lower temperatures (Fig. 1c).

Interestingly, here we have a drift-diffusion problem where a Brownian particle is subject to a time-independent potential $\tilde{V}_b(x)$, as sketched in Fig. 1a. $\tilde{V}_b(x)$ differs from the ideal potential $V_b(x) \approx -\mathcal{E}_{\text{tot},z} d_{b,z}$ mentioned above because of the periodic boundary conditions in our simulations and the fact that e-bubbles are not point dipoles. Nevertheless, $\tilde{V}_b(x)$ can be expected to have an approximately linear dependence with x in the central region of the supercell, resulting in a constant drift force $\tilde{f}_{b,x}(x) \propto \mathcal{E}_z^{(1)}$ acting on the bubble. As argued in Supplementary Note 1, within that constant-drift region we expect $\mathcal{P}(x)$ to satisfy a simplified Smoluchowski equation [27],

$$c \frac{\partial \mathcal{P}(x)}{\partial x} + D \frac{\partial^2 \mathcal{P}(x)}{\partial x^2} = 0, \quad (3)$$

where c is the drift velocity and D the diffusion constant

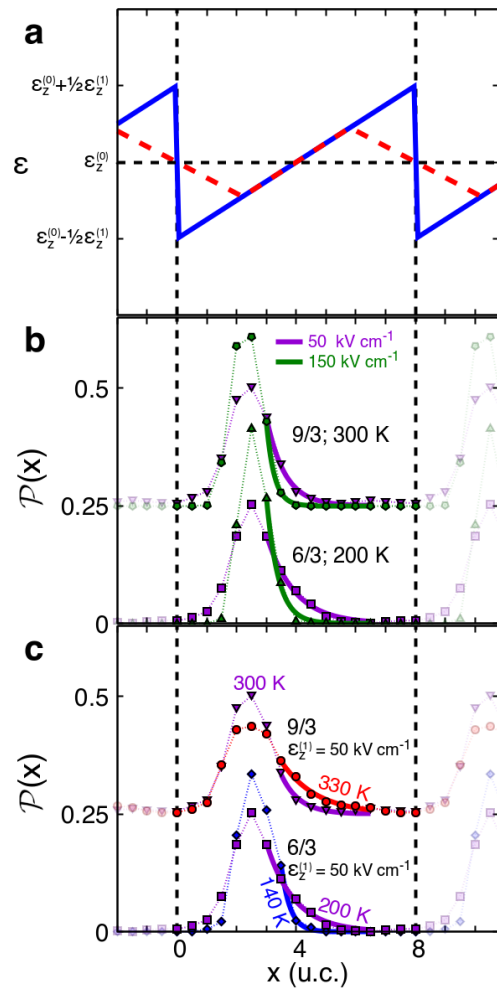


FIG. 1: **Confined e-bubbles under the action of a sawtooth-modulated electric field.** In panel a, the blue solid line shows the variation with x of the sawtooth-modulated electric field, in a periodically-repeated supercell with a length of $N = 8$ perovskite units. The red dashed line is proportional to the electric potential (\tilde{V}_b) experienced by an e-bubble of 4 unit cells in diameter, as caused by the applied field (blue). Panels b and c show the probability distribution for the e-bubble position ($\mathcal{P}(x)$) for varying modulation amplitude and temperature, respectively. In each panel, the top lines correspond to the 9/3 superlattice (-2% epitaxial strain, $\mathcal{E}_z^{(0)} = 1.0 \text{ MV cm}^{-1}$) while the bottom lines pertain to the 6/3 system (no epitaxial strain, $\mathcal{E}_z^{(0)} = 1.5 \text{ MV cm}^{-1}$). Symbols correspond to computed data, thin dotted lines are guides to the eye, and solid thick lines are fits to Eq. (4).

of the Brownian bubble. This equation is solved for

$$\mathcal{P}(x) = A \exp\left(-\frac{c}{D}x\right), \quad (4)$$

where A is an integration constant. We thus expect $\mathcal{P}(x)$ to approach zero exponentially fast as we move into the right half of the supercell, the decay being controlled by c/D .

As shown in Fig. 1, we can fit well the tails of the com-

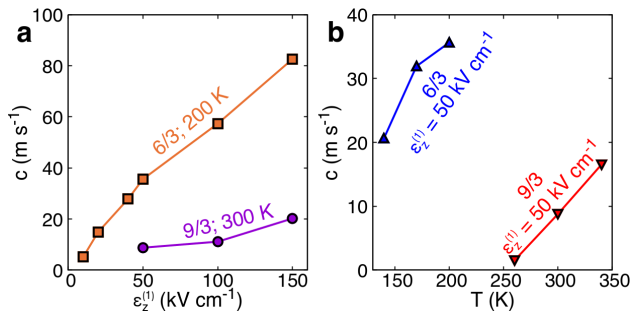


FIG. 2: **Predicted e-bubble velocities under static bias.** The drift velocities obtained by fitting to Eq. (4) grow as we increase the amplitude of the sawtooth modulation (a) or the temperature (b). The results correspond, essentially, to the cases displayed in Fig. 1.

puted $\mathcal{P}(x)$ probability densities using Eq. (4), and thus obtain the corresponding c/D ratios. Using D obtained from MD simulations with $\mathcal{E}_z^{(1)} = 0$, we can calculate the velocities c . Our results, summarized in Figure 2, show an approximate proportionality between c and $\mathcal{E}_z^{(1)}$ (as expected; see Supplementary Note 1) and a significant T dependence. Remarkably, we predict e-bubble velocities over 20 m/s.

This indirect approach to estimate the bubble velocity c may seem tenuous. Can we actually observe e-bubbles moving at 20 m/s in our simulations? To answer this, we now consider a time-dependent electric field of the form

$$\mathcal{E}_{\text{tot},z}(x;t) = \mathcal{E}_z^{(0)} + \mathcal{E}_z^{(1)} \sin\left(\frac{2\pi}{L}x - \frac{2\pi}{\tau}t\right). \quad (5)$$

Here, τ is the time it takes the sinusoidal perturbation to complete a full oscillation; hence, $v_W = L/\tau$ is the field-wave velocity. Noting that we work with $L \approx 8 \times 3.9 \text{ \AA}$, a field wave propagating at 20 m/s corresponds to $\tau \approx 150 \text{ ps}$, a time scale within the scope of our second-principles calculations [9].

We thus consider waves with amplitudes $\mathcal{E}_z^{(1)}$ within 20% of the homogeneous component $\mathcal{E}_z^{(0)}$, and τ 's between 10 ps and 1000 ps. The results in Figure 3 illustrate the three different situations we find: bubbles following comfortably a slow wave (green), bubbles having trouble to follow a faster wave and getting off track occasionally (blue), and bubbles incapable of keeping up with very fast waves (red). These regimes can be best appreciated in Supplementary Movies 1 to 3, respectively.

Figure 4 shows the average e-bubble velocity, c , against the wave velocity v_W . In the representative case of the 6/3 superlattice, we find $c \approx v_W$ at small wave velocities. This perfect tracking regime extends up to about 50 m/s for a relatively small perturbation with $\mathcal{E}_z^{(1)} = 50 \text{ kV cm}^{-1}$, and up to about 150 m/s for $\mathcal{E}_z^{(1)} = 100 \text{ kV cm}^{-1}$. Then, c always reaches a maximum beyond which the bubbles slow down considerably. We

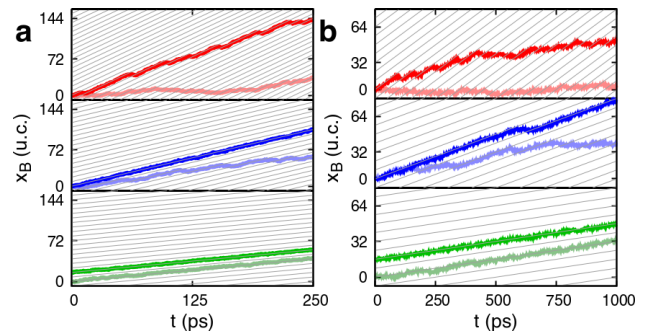


FIG. 3: **Simulated e-bubble motion driven by a field wave.** Bubble position (x_B) as a function of time. Representative results for 6/3 and 9/3 superlattices are shown in panels a and b, respectively. In every subpanel, the data shown with brighter colors correspond to a wave amplitude $\mathcal{E}_z^{(1)} = 100 \text{ kV cm}^{-1}$, while dim colors are used for $\mathcal{E}_z^{(1)} = 50 \text{ kV cm}^{-1}$. The background lines track the motion of the minima of the sinusoidal field modulation; such minima correspond to regions where the e-bubble has a lower potential energy. For slow waves (bottom subpanels, green lines) the e-bubbles follow the field wave, even for modulations of small amplitude. As the waves get faster (medium and top subpanels), the e-bubbles begin to get off track sometimes, to the point that they may become nearly immobile (see cases in dim red, top subpanels).

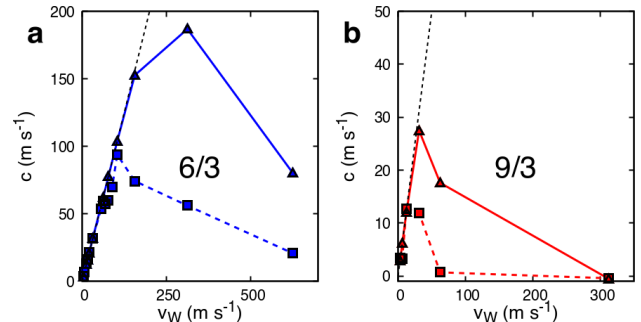


FIG. 4: **Predicted e-bubble velocities under a field wave.** We show results for our model 6/3 (a) and 9/3 (b) superlattices, using solid and dashed lines for wave modulations with $\mathcal{E}_z^{(1)} = 100 \text{ kV cm}^{-1}$ and $\mathcal{E}_z^{(1)} = 50 \text{ kV cm}^{-1}$, respectively. The black dashed line corresponds to a perfect tracking, where $c = v_W$. The results yield a clear qualitative picture; note, though, that obtaining good statistics in the regime where $c \lesssim v_W$ would require prohibitively long simulations, as in such cases the bubbles' slip-offs are rare events.

obtain maximum bubble speeds of about 180 m/s and 30 m/s, respectively, for the 6/3 superlattice at 200 K and the 9/3 superlattice at 300 K. We thus ratify the prediction of fast e-bubble currents. Remarkably, the bubbles remain stable throughout the simulations, even when they are dazed by fast field waves, which confirms their resilience as long-lived quasiparticles.

It thus seems that field waves allow us to drag e-bubbles faster than static gradients do. The reason is

simple: for the same $\mathcal{E}_z^{(1)}$, the field waves exert on the bubbles a force (given essentially by the x -derivative of Eq. (5)) that can be up to 2π times larger than the maximum force caused by the field gradient (Eq. (2)).

When are the waves too fast for the e-bubbles to follow? Recall that e-bubbles move by switching dipoles at their boundary; hence, their velocity is ultimately limited by the speed of such a local polarization switching. A bubble velocity of 100 m/s implies that boundary cells switch in about 4 ps. This may seem surprisingly fast; yet, it is consistent with atomistic studies of ferroelectric switching in PTO [28]. Moreover, the authors of Ref. 28 found that field-driven domain wall motion in PTO proceeds through the formation of a critical nucleus of about 3×3 unit cells. Noting that the switching of interest here involves only a few boundary cells, it is conceivable it will typically comprise a single nucleation event, thus being ultrafast.

Hence, while intriguing aspects of the simulated bubble currents remain for future study (e.g., concerning the T -dependence of c), our basic results seem physically sound and yield a clear picture. In Supplementary Note 2 and Supplementary Figures S1 to S3 we present additional results further supporting our main conclusions.

The cases simulated here are admittedly challenging (we are restricted by the excessive computational cost of treating bigger systems); yet, we believe they fall within the range of what is experimentally conceivable. For example, it may be possible to create suitable static field gradients by using wedge-shaped electrodes, taking advantage of advances in nanofabrication [29]. Also, progress on surface acoustic waves suggests that field waves propagating at hundreds of m/s with wavelenghts of tens of nm may soon be within reach [30]. Pinning, though, will constitute an unavoidable difference between our defect-free simulations and experiments. Pinning will reduce the number of mobile bubbles and slow down the ones that can move. Nevertheless, we see no reason to believe that all e-bubbles will be clamped in high-quality samples – note e.g. the experimental results of Ref. [22], which suggest stochastic dynamics of ferroelectric domains. Hence, we think that ultimately pinning will not be an unsurmountable problem.

We conclude by noting that, typically, magnetic skyrmions can be accelerated to about 100 m/s, and only recently [31] have there been reports of higher speeds (900 m/s). Notwithstanding the differences between our theoretical e-bubbles and the magnetic skyrmions actually measured, it is remarkable that our predictions – where no velocity optimization was attempted – yield results on par with record-setting magnetic systems. Hence, our calculations suggest that e-bubbles may become a quasiparticle of choice in applications where magnetic skyrmions are being considered, e.g. for ultralow-power neuromorphic computing. We hope these results will attract the attention of physicists and engineers alike,

as they may herald an exciting era of research – fundamental and applied – focused on electric-bubble currents.

Methods

Second-principles simulations are performed using the SCALE-UP package [21, 32, 33] and the same approach as in previous studies of PTO/STO superlattices [6, 22, 23]. The superlattice models are based on potentials for the pure bulk compounds – fitted to first-principles results [21] – and adjusted for the superlattices [22]. The e-bubble simulations and analysis (e.g., definition of e-bubble centers, quantification of their trajectories) follow the methodology described in Ref. 9. The only noteworthy differences pertain to the MD simulations with electric-field waves. In such cases, we first prepare a thermalized state (atomic positions and velocities) by running an isokinetic MD simulation of the material under the action of a static wave-modulated electric field (i.e., as obtained from Eq. (5) for $t = 0$). Then, we turn on the motion of the electric field wave and simulate the system dynamics by simply following Newton's equations of motion. Note, though, that here we have a time-dependent potential, so the total energy of the system is not conserved. To keep the temperature at its desired value, we thermostat the system by applying a suitable velocity rescaling every 50 ps. We explicitly check that such a rescaling has no significant effect on the e-bubble diffusion. All our MD simulations with sawtooth-modulated fields run for at least 3 ns, which we find is enough to get reliable results for $\mathcal{P}(x)$. All our MD simulations with field waves run for at least 1 ns.

Acknowledgements

Work funded by the Luxembourg National Research Fund (FNR), mainly through grant C21/MS/15799044/FERRODYNAMICS and also through grant C23/MS/17909853/BUBBLACED. We are thankful for inspiring discussions with the members of the TOPOCOM Marie Skłodowska-Curie Doctoral Network, particularly D.R. Rodrigues (Bari).

-
- [1] C. Lichtensteiger, S. Fernandez-Pena, C. Weymann, P. Zubko, and J.-M. Triscone, *Nano Letters* **14**, 4205 (2014).
 - [2] Q. Zhang, L. Xie, G. Liu, S. Prokhorenko, Y. Nahas, X. Pan, L. Bellaiche, A. Gruverman, and N. Valanoor, *Advanced Materials* **29**, 1702375 (2017).
 - [3] S. R. Bakaul, S. Prokhorenko, Q. Zhang, Y. Nahas, Y. Hu, A. Petford-Long, L. Bellaiche, and N. Valanoor, *Advanced Materials* **33**, 2105432 (2021).
 - [4] S. Prokhorenko, Y. Nahas, V. Govinden, Q. Zhang, N. Valanoor, and L. Bellaiche, *Nature Communications* **15**, 412 (2024).
 - [5] L. Bastogne, F. Gómez-Ortiz, S. Anand, and P. Ghosez, *Nano Letters* **24**, 13783 (2024).

- [6] S. Das, Y. L. Tang, Z. Hong, M. A. P. Gonçalves, M. R. McCarter, C. Klewe, K. X. Nguyen, F. Gómez-Ortiz, P. Shafer, E. Arenholz, et al., *Nature* **568**, 368 (2019).
- [7] M. A. Pereira Gonçalves, C. Escorihuela-Sayalero, P. García-Fernández, J. Junquera, and J. Íñiguez, *Science Advances* **5**, eaau7023 (2019).
- [8] L. Han, C. Addiego, S. Prokhorenko, M. Wang, H. Fu, Y. Nahas, X. Yan, S. Cai, T. Wei, Y. Fang, et al., *Nature* **603**, 63 (2022).
- [9] H. Aramberri and J. Íñiguez-González, *Phys. Rev. Lett.* **132**, 136801 (2024).
- [10] J. Junquera, Y. Nahas, S. Prokhorenko, L. Bellaiche, J. Íñiguez, D. G. Schlom, L.-Q. Chen, S. Salahuddin, D. A. Muller, L. W. Martin, et al., *Rev. Mod. Phys.* **95**, 025001 (2023).
- [11] F. Peper, J. Lee, J. Carmona, J. Cortadella, and K. Morita, *J. Emerg. Technol. Comput. Syst.* **9** (2013).
- [12] D. Pinna, F. Abreu Araujo, J.-V. Kim, V. Cros, D. Querlioz, P. Bessiere, J. Droulez, and J. Grollier, *Phys. Rev. Appl.* **9**, 064018 (2018).
- [13] J. Grollier, D. Querlioz, K. Y. Camsari, K. Everschor-Sitte, S. Fukami, and M. D. Stiles, *Nature Electronics* **3**, 360 (2020).
- [14] J. Kaiser and S. Datta, *Applied Physics Letters* **119**, 150503 (2021).
- [15] K. Raab, M. A. Brems, G. Beneke, T. Dohi, J. Rothörl, F. Kammerbauer, J. H. Mentink, and M. Kläui, *Nature Communications* **13**, 6982 (2022).
- [16] C. Cortes and V. Vapnik, *Machine Learning* **20**, 273 (1995).
- [17] T. Yokouchi, S. Sugimoto, B. Rana, S. Seki, N. Ogawa, Y. Shiomi, S. Kasai, and Y. Otani, *Science Advances* **8**, eabq5652 (2022).
- [18] G. Finocchio, J. A. C. Incorvia, J. S. Friedman, Q. Yang, A. Giordano, J. Grollier, H. Yang, F. Ciubotaru, A. V. Chumak, A. J. Naemi, et al., *Nano Futures* **8**, 012001 (2024).
- [19] F. Jonietz, S. Mühlbauer, C. Pfleiderer, A. Neubauer, W. Münzer, A. Bauer, T. Adams, R. Georgii, P. Böni, R. A. Duine, et al., *Science* **330**, 1648 (2010).
- [20] N. Nagaosa and Y. Tokura, *Nature Nanotechnology* **8**, 8579 (2013).
- [21] J. C. Wojdeł, P. Hermet, M. P. Ljungberg, P. Ghosez, and J. Íñiguez, *Journal of Physics: Condensed Matter* **25**, 305401 (2013).
- [22] P. Zubko, J. C. Wojdeł, M. Hadjimichael, S. Fernandez-Pena, A. Sené, I. Luk'yanchuk, J. Triscone, and J. Íñiguez, *Nature* **534**, 524 (2016).
- [23] P. Shafer, P. García-Fernández, P. Aguado-Puente, A. R. Damodaran, A. K. Yadav, C. T. Nelson, S.-L. Hsu, J. C. Wojdeł, J. Íñiguez, L. W. Martin, et al., *Proceedings of the National Academy of Sciences* **115**, 915 (2018).
- [24] M. Graf, H. Aramberri, P. Zubko, and J. Íñiguez, *Nature Materials* **21**, 1252 (2022).
- [25] F. Gómez-Ortiz, M. Graf, J. Junquera, J. Íñiguez-González, and H. Aramberri, *Phys. Rev. Lett.* **133**, 066801 (2024).
- [26] E. Raimondo, E. Saugar, J. Barker, D. Rodrigues, A. Giordano, M. Carpentieri, W. Jiang, O. Chubykalo-Fesenko, R. Tomasello, and G. Finocchio, *Phys. Rev. Appl.* **18**, 024062 (2022).
- [27] V. Balakrishnan, *Elements of Nonequilibrium Statistical Mechanics* (Springer and ANE Books Pvt. Ltd., 2021), ISBN 9783030622329.
- [28] Y.-H. Shin, I. Grinberg, I.-W. Chen, and A. M. Rappe, *Nature* **449**, 881 (2007).
- [29] E. Berenschot, R. M. Tiggelaar, B. Borgelink, C. van Kampen, C. S. Deenen, Y. Pordeli, H. Witteveen, H. J. G. E. Gardeniers, and N. R. Tas, *ACS Applied Nano Materials* **5**, 15847 (2022).
- [30] P. Delsing, A. N. Cleland, M. J. A. Schuetz, J. Knörzer, G. Giedke, J. I. Cirac, K. Srinivasan, M. Wu, K. C. Balram, C. Bäuerle, et al., *Journal of Physics D: Applied Physics* **52**, 353001 (2019).
- [31] V. T. Pham, N. Sisodia, I. D. Manici, J. Urrestarazu-Larrañaga, K. Bairagi, J. Pelloux-Prayer, R. Guedas, L. D. Buda-Prejbeanu, S. Auffret, A. Locatelli, et al., *Science* **384**, 307 (2024).
- [32] P. García-Fernández, J. C. Wojdeł, J. Íñiguez, and J. Junquera, *Physical Review B* **93**, 195137 (2016).
- [33] *SCALE-UP, an implementation of second-principles density functional theory*, <https://www.secondprinciples.unican.es/>.